

# Basalts of a Seamount on the Eastern Flank of the Charlie Gibbs Transform Fracture Zone, North Atlantic: Petrochemical and Isotopic Evidence of a Microplume-Affected Formation in the Axial Zone of the Mid-Atlantic Ridge

S. G. Skolotnev<sup>a,\*</sup>, A. A. Peyve<sup>a</sup>, S. A. Dokashenko<sup>a</sup>, V. N. Dobrolyubov<sup>a</sup>,  
O. I. Okina<sup>a</sup>, and B. V. Ermolaev<sup>a</sup>

Presented by Academician K.E. Degtyarev August 10, 2023

Received August 10, 2023; revised August 28, 2023; accepted August 30, 2023

**Abstract**—The composition of basalts dredged from the slopes of a single seamount (guyot), which is located south of the eastern end of the Charlie Gibbs Fracture Zone in the North Atlantic, is studied. Groups of high- and low-Ti rocks, which belong to oceanic tholeiites of the E-MORB and T-MORB types, respectively, are recognized. The first group of basalts have higher contents of TiO<sub>2</sub>, Na<sub>2</sub>O, K<sub>2</sub>O, P<sub>2</sub>O<sub>5</sub>, Fe<sub>2</sub>O<sub>3</sub>, and incompatible trace elements. The basalts of both groups are similar in the normalized lithophile element patterns indicating their melting from a similar mantle substrate. The difference in their composition is probably caused by melting of high-Ti volcanic rocks at a deeper intermediate level between spinel and garnet facies. Our studies give grounds to believe that the seamount also formed as a large neovolcanic rise 64–67 Ma ago under the influence of a microplume, which was a branch of the Milne deep mantle plume.

DOI: 10.1134/S1028334X23602195

## INTRODUCTION

Following J.T. Wilson [1], the origin of chains of seamounts and linear tectono-volcanic rises and ridges, which are abundant on the seafloor, is considered by most researchers a result of magmatic activity of hot spots, which form at a sublithospheric level of the upper mantle under an ascending deeper mantle plume, probably from the core–mantle boundary. The reasons for the formation of single volcanic seamounts are less evident. One of these nameless seamounts was found in the 50<sup>th</sup> cruise of R/V *Akademik Nikolai Strakhov* in the North Atlantic (Fig. 1) and was studied using bathymetric and hydromagnetic survey.

According to the study, this morphostructure, named seamount 51-19, is a guyot (Fig. 1), which rises above the seafloor for 1500 m and its flat summit reaches a depth of 2500 m [3]. The guyot with coordinates of the summit center of the 51°15' N and 19°35' E is longitudinally elongated for 18 km. It is located east of the Eastern Thule Rise directly to the

south from the eastern end of the Charlie Gibbs Fracture Zone (Fig. 1). The processing of the results of a hydromagnetic survey allowed the authors of [3] to conclude that seamount 51-19 formed near or in the axial spreading zone of the Mid-Atlantic Ridge (MAR) about 64–67 Ma ago.

Additional data on the origin of the seamount are provided by the composition of basalts dredged from the slopes of this seamount in the 53<sup>th</sup> cruise of R/V *Akademik Sergei Vavilov* [4] and are presented in this paper.

Basalts as small rubble were dredged at two stations V5333 and V5334 from the eastern slope of the seamount at a depth of 3150–2600 m (Fig. 1); their coordinates are given in Supplementary 1 (Table S1).

The basalts are the aphyric and rare small-porphyrical varieties. Phenocrysts 1–5 mm across, the amount of which are 1–3 vol %, include plagioclase and less often clinopyroxene and olivine. The main mass of the rock, as a rule, is fully crystalline and is composed of plagioclase and clinopyroxene grains and rare olivine and an opaque ore mineral (up to 1 vol %). In some samples (V5333/2, 16, V5334/4, 5), the amount of ore mineral increases up to 2–3 vol %. Except for several samples, the secondary minerals are rare (0–3 vol %) and include an olive clay mineral,

<sup>a</sup> Geological Institute, Russian Academy of Sciences, Moscow, 119117 Russia

\*e-mail: sg\_skol@mail.ru

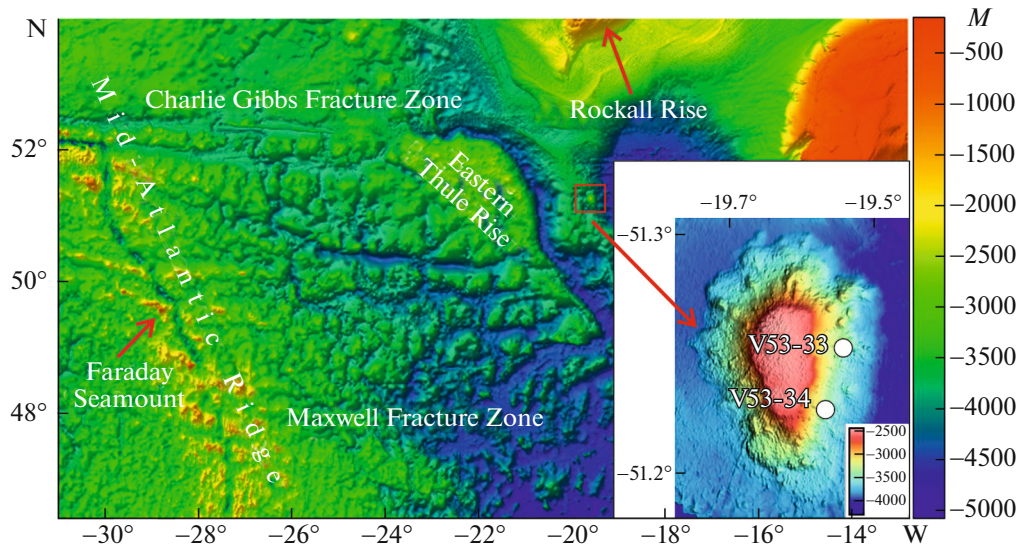


**Fig. 1.** Seafloor structure between the Maxwell and Charlie Gibbs fracture zones based on GEBCO map [2]. The position of seamount 51-19 is noted by a red square. The depth scale is given from the right. The inset shows the bathymetric map of the seamount and the position of the dredge stations from [3]; the depth scale (m) is shown in the lower right-hand corner of the inset.

locally, mixed with Fe hydroxides. Sample V5234/2 contains abundant chlorite (up to 20 vol %). In sample V5234/3, plagioclase microlites are significantly replaced by albite and K-feldspar. The volcanic rocks are weakly porous excluding sample V5333/7. The amount of small pores (up to 0.25 mm in diameter) does not exceed 1 vol %. Sample V5333/7 hosts abundant empty vesicles (up to 15 vol %) up to 10 mm across.

### ANALYTICAL METHODS

The chemical composition of basalts was determined at the Geological Institute, Russian Academy of Sciences (GIN RAS, Moscow). The bulk rock composition was analyzed using X-ray fluorescence on a S4 Pioneer X-Ray spectrometer (Bruker, Germany). The trace element content of basalts was determined using inductively coupled plasma mass spectrometry (ICP-MS) on an Element2 mass spectrometer (Thermo Fisher Scientific GmbH, Germany) following the methodology of [5]. The isotopic composition of volcanic rocks was analyzed at the Center for Isotopic Studies, Russian Geological Research Institute (VSEGEI) of the Ministry of Natural Resources and Ecology of the Russian Federation (St. Petersburg) following the methodology of [6]. The bulk composition of basalts is given in Supplementary 1 (Table S1).

The studied basalts are subdivided on two petrochemical groups: low-Ti (samples V5333/5-7) and high-Ti (samples V5333/2,16, V5334/4,5). The high-Ti group has higher contents of  $\text{TiO}_2$  (2.67–4.36 and 1.49–1.86%),  $\text{Na}_2\text{O}$  (2.65–2.73% and 2.22–2.61%),  $\text{K}_2\text{O}$  (0.31–0.49 and 0.12–0.18 wt %),  $\text{P}_2\text{O}_5$  (0.21–0.29

and 0.10–0.13 wt %), and  $\text{Fe}_2\text{O}_3$  (14.71–16.86 and 11.66–15.18 wt %) and lower contents of  $\text{Al}_2\text{O}_3$  (10.43–13.39 and 13.58–16.10 wt %),  $\text{MgO}$  (4.09–5.20 and 4.92–6.69 wt %), and  $\text{CaO}$  (9.44–10.67 and 11.14–12.62 wt %). In the  $\text{MgO}$ – $\text{TiO}_2$ ,  $\text{Na}_2\text{O}$ ,  $\text{K}_2\text{O}$ , and  $\text{P}_2\text{O}_5$  diagrams (Figs. 2a–2d), the basalts from each group form independent fields and the  $\text{TiO}_2$ ,  $\text{Na}_2\text{O}$ , and  $\text{K}_2\text{O}$  contents of each group consecutively increase with a decreasing  $\text{MgO}$  content. In the  $\text{MgO}$ – $\text{Al}_2\text{O}_3$  and  $\text{CaO}$  diagrams (Figs. 2e, 2f), the studied samples form common fields with the  $\text{MgO}$  content decreasing from 6.69 to 4.09 wt % and a corresponding decrease in the  $\text{Al}_2\text{O}_3$  and  $\text{CaO}$  content.

The trace element content of basalts is given in Supplementary 1 (Table S2) and shows that the high-Ti volcanic rocks differ significantly from low-Ti basalts in the higher content of incoherent elements such as Rb (5.2–8.1 and 2.3 ppm), Ba (84–136 and 22 ppm), Th (1.08–1.63 and 0.31 ppm), Nb (14–24 and 6.3 ppm), U (0.31–0.47 and 0.083 ppm), La (12–19 and 4.7 ppm), Pb (1.40–1.51 and 0.51 ppm), Sr (257–411 and 145 ppm), Zr (173–202 and 65 ppm), and Hf (4.1–4.5 and 1.67 ppm), as well as the higher V content (407–471 and 321 ppm) and lower Cr content (60–212 and 322 ppm), whereas the contents of Ni (60–111 ppm), Co (50 ppm), and Y (21–30 ppm) are similar in both groups.

The chondrite-normalized REE pattern of the low-Ti sample V5233/5 is almost parallel to axis  $x$  at a level of ten of the normalized values:  $(\text{La}/\text{Sm})_n = 1.21$ ,  $(\text{Sm}/\text{Yb})_n = 1.18$  (Fig. 3a). The high-Ti samples V5234/4 and V5234/5 exhibit a consecutive increase from heavy to light REEs:  $(\text{La}/\text{Sm})_n = 1.28$ –1.58,  $(\text{Sm}/\text{Yb})_n = 1.78$ –2.42. According to the character of

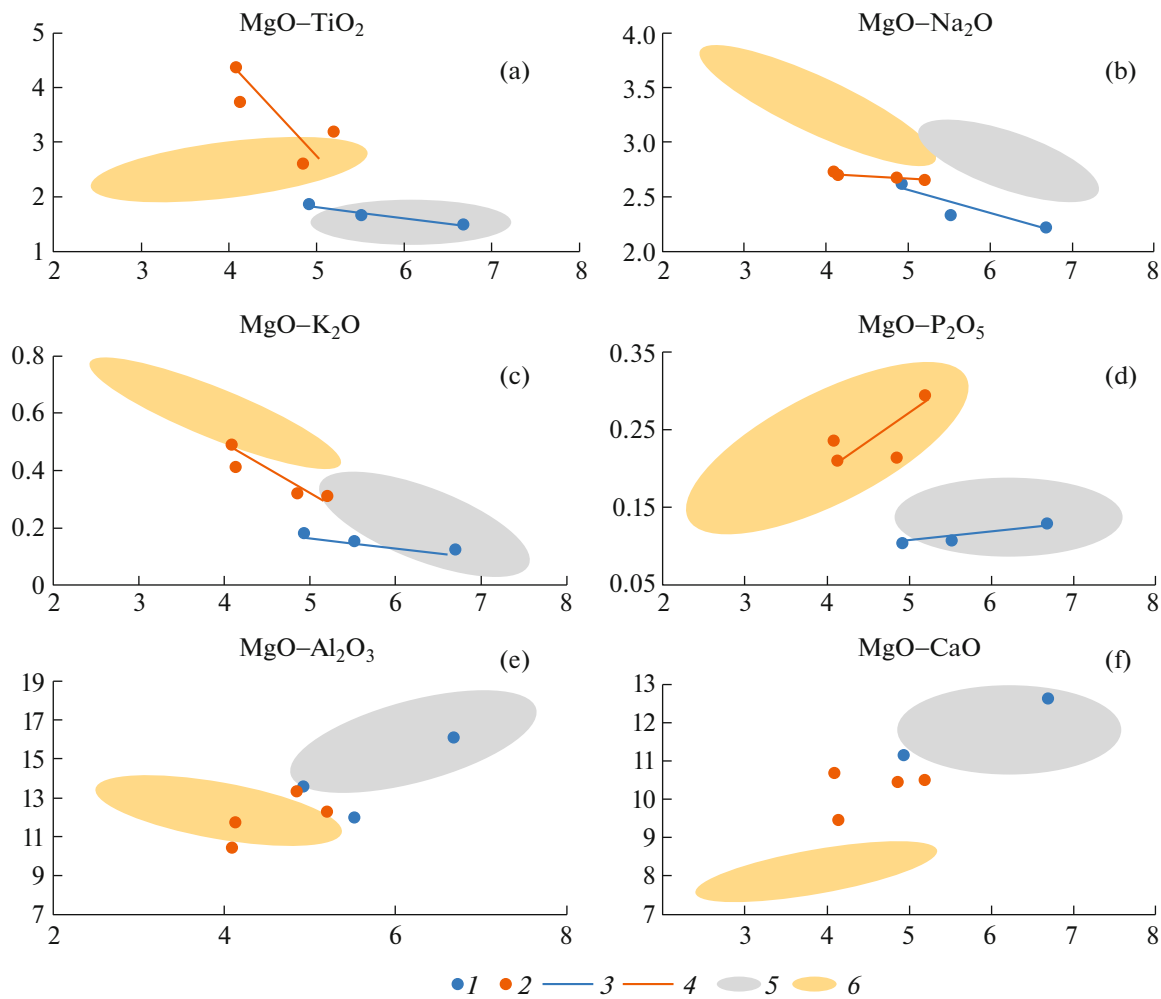


**Fig. 2.** Correlation between the  $\text{TiO}_2$ ,  $\text{Na}_2\text{O}$ ,  $\text{K}_2\text{O}$ ,  $\text{P}_2\text{O}_5$ ,  $\text{Al}_2\text{O}_3$ , and  $\text{CaO}$  content (wt %) and the  $\text{MgO}$  content (wt %). 1, 2, Basalts of low-Ti (1) and high-Ti (2) groups; 3, 4, trends of variation of composition of basalts of low-Ti (3) and high-Ti (4) groups; 5, 6, fields of composition of basalts from the axial MAR part between the Maxwell and Charlie Gibbs fracture zones (original data): 5, T-MORB type; 6, E-MORB type.

the REE pattern and the  $(\text{La}/\text{Sm})_n$  ratio, the low-Ti basalts could be ascribed to T-MORB oceanic tholeiites, whereas the high-Ti basalts belong to E-MORBs [7]. According to the  $(\text{Sm}/\text{Yb})_n$  ratio, the low-Ti basalts were melted at the spinel facies level, whereas the high-Ti basalts were melted in a deeper horizon at an intermediate level between the spinel and garnet facies [8].

The character of spider-diagrams of both basaltic groups is similar except for the lower pattern level of the low-Ti sample (Fig. 3b). The pattern lines rise from La further to more incoherent Nb ( $(\text{Nb}/\text{La})_n = 1.13\text{--}1.32$ ) and then decrease to Th. In high-Ti samples, the pattern decreases further to Rb, but forms a positive Ba anomaly, whereas the normalized Rb and Ba values of the low-Ti basalt are similar to those of Th. All patterns exhibit negative U and Pb anomalies. The analysis of spider-diagrams shows that the mantle substrate, which yielded basalts of both groups, had a

similar composition. In accordance with [10], the positive  $(\text{Nb}/\text{La})_n$  values indicate the presence of a HIMU mantle component in the substrate, whereas the higher normalized Ba (and locally Rb) values indicate the presence of the enriched mantle (EM).

The  $^{87}\text{Sr}/^{86}\text{Sr}$ ,  $^{143}\text{Nd}/^{144}\text{Nd}$ ,  $^{206}\text{Pb}/^{204}\text{Pb}$ ,  $^{207}\text{Pb}/^{204}\text{Pb}$ , and  $^{208}\text{Pb}/^{204}\text{Pb}$  values were determined in two samples of high-Ti basalts (V5234/4 and V5234/5), and they are shown in Supplementary 1 (Table S3). The analysis of the position of isotope ratios of the studied samples in variation diagrams (Fig. 4) shows that they are similar and correspond to the compositional fields of rocks of the Iceland Rise [11].

In the  $^{206}\text{Pb}/^{204}\text{Pb}$ – $^{207}\text{Pb}/^{204}\text{Pb}$  diagram, the data points occur approximately in the middle part of the line, which connects the DM (depleted mantle) and HIMU mantle sources [12] (Fig. 4a), which supports the geochemical data on the involvement of the

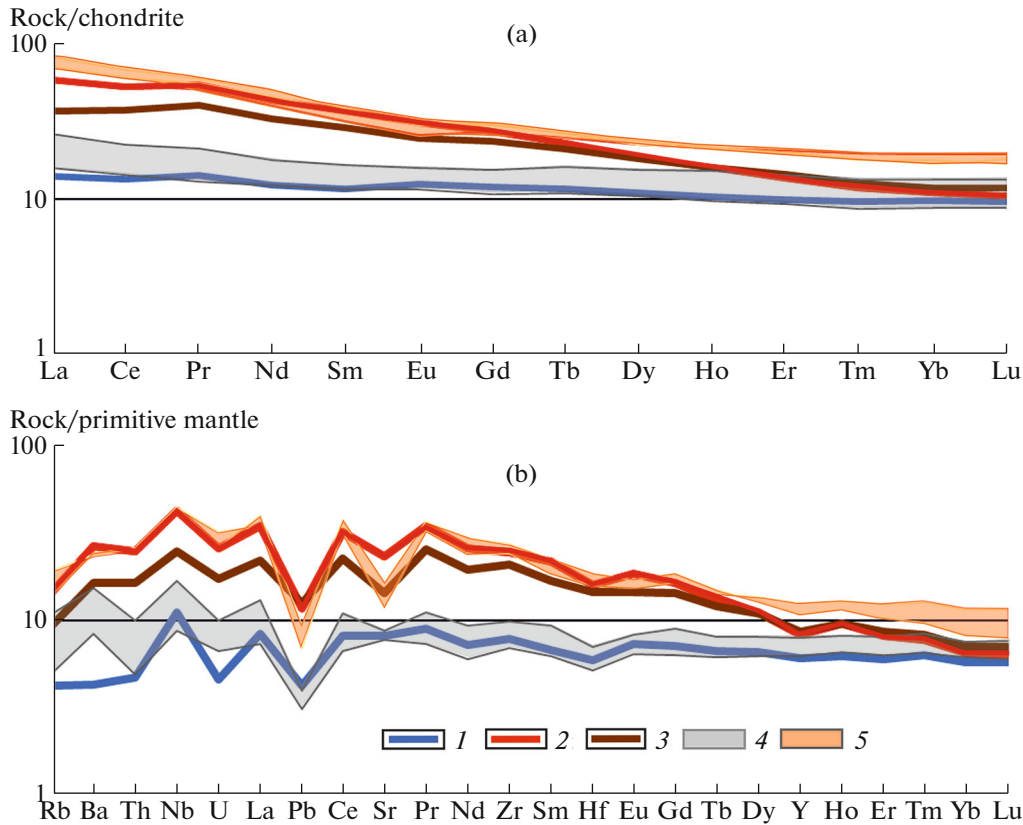


**Fig. 3.** Trace element patterns: (a) REE patterns normalized after chondrite [7]; (b) trace element spider-diagrams normalized after the primitive mantle [9]. (1) Sample V5333/5; (2) sample V5334/4; (3) sample V5334/5; (4, 5) pattern fields of basalts from the axial MAR part between the Maxwell and Charlie Gibbs fracture zones (original data); (5) T-MORB type; (6) E-MORB type.

HIMU mantle source in the melting substrate. In the  $^{87}\text{Sr}/^{86}\text{Sr}$ – $^{143}\text{Nd}/^{144}\text{Nd}$  diagram (Fig. 4b), the samples are located in a triangle with apices for the DM, HIMU, and EM-2 compositions [12], which indicates the presence of the EM-2 mantle source in the studied basalts (although in minor amount). Thus, the isotopic data show that the mantle substrate of basalts of seamount 51-19 is a mixture of the DM, HIMU, and, to a lesser extent, EM-2 mantle sources.

## DISCUSSION AND CONCLUSIONS

In summarizing the analytical study of basalts, it can be concluded that they contain two petrochemical groups: high-Ti with a higher content of  $\text{TiO}_2$ ,  $\text{Na}_2\text{O}$ ,  $\text{K}_2\text{O}$ ,  $\text{P}_2\text{O}_5$ ,  $\text{Fe}_2\text{O}_3$ , and incoherent trace elements and low-Ti, which correspond to E-MORB and T-MORB oceanic tholeiites, respectively. These rocks often occur within the MAR. In spite of the different composition, the basalts of both groups were melted from a compositionally similar substrate, which is typical of mantle affected by the Iceland plume [11]. It is most likely that their compositional differences are caused by different melting depths of their parental melts, which was greater for the high-Ti basalts with higher

$(\text{Sm}/\text{Yb})_n$  values (at the intermediate level between spinel and garnet facies), that probably resulted in a lower degree of partial melting of the mantle substrate (higher  $(\text{La}/\text{Sm})_n$  values of high-Ti basalts).

The variations in the composition of the studied basalts also depend on the processes of fractional crystallization of their parental melts: under consecutive crystallization of olivine, sodic plagioclase, and clinopyroxene, the residual melt was depleted in Mg, Al, and Ca and was enriched in Ti, Na, K, and Fe. At the same time, it is evident that only processes of fractional crystallization could not explain the differences in the composition of both basaltic groups, because the high-Ti basalts have higher  $\text{TiO}_2$ ,  $\text{Na}_2\text{O}$ ,  $\text{K}_2\text{O}$ , and  $\text{P}_2\text{O}_5$  contents at a similar MgO content (Figs. 2a, 2c, 2d). In high-Ti basalts, the increase in MgO content is accompanied by a decrease in the  $\text{P}_2\text{O}_5$  content (Fig. 2d) indicating the fractionation of apatite from their melts.

Our data on the composition of basalts of seamount 51-19 allow us to refine the origin. Basalts with similar petro-geochemical and isotopic parameters (Fig. 4) were recently found relatively close to this seamount in axial and crest MAR zones between the Maxwell and Charlie Gibbs fracture zones, and they also contain both low- and high-Ti types. The content

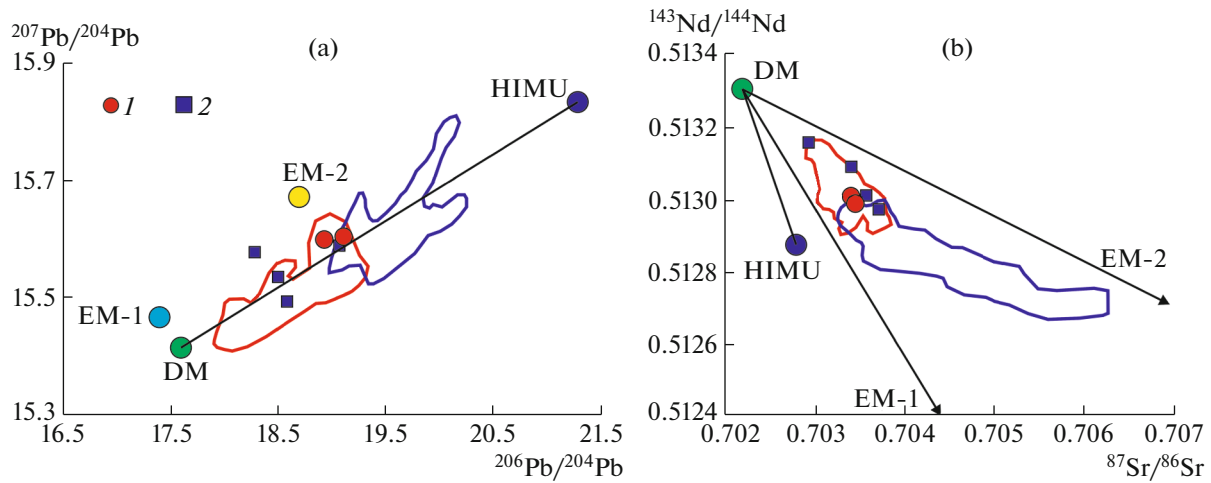


**Fig. 4.** Diagrams of variation of isotope ratios. (1) Basalts of seamount 51-19; (2) basalts from the axial MAR part between the Maxwell and Charlie Gibbs fracture zones (original data). Red and blue lines mark the compositional field of basalts of the Iceland Rise and Azores Rise after [11]. Black lines connect the isotopic compositions of mantle sources DM, HIMU, EM-1, and EM-2 after [12].

of  $\text{TiO}_2$ ,  $\text{Al}_2\text{O}_3$ ,  $\text{K}_2\text{O}$ , and  $\text{P}_2\text{O}_5$  (Figs. 2a, 2c, 2d, 2e), and some incoherent elements (Fig. 3) are quite similar. The high- and low-Ti basalts (E-MORBs and T-MORBs, respectively) between the Maxwell and Charlie Gibbs fracture zones compose large volcanic edifices, in particular, the Faraday Seamount (Fig. 1), which formed as large neovolcanic rises in the axial spreading zone [13]. A paper dedicated to this rise is in press. About 64–67 Ma ago, seamount 51-19 could also have been a similar edifice, which is supported by the paleomagnetic and bathymetric data published in [13]. Similar large volcanic edifices often occur along the axial MAR zone and are mostly related to the uplift of enriched mantle microplumes, the origination of which is caused either by sublateral or subvertical branches of closely located large deep mantle plumes [14, 15].

Seamount 51-19 is located at the latitude of the Eastern Thule Rise, east of it [2] symmetrical to the Western Thule Rise in the western MAR flank. This gives grounds for the authors of [16] to suggest that 54–46 Ma ago two uplifts were a common structure, which formed in the axial MAR spreading zone as a result of subaxial uplift of the deep mantle plume. According to one scenario, the formation of the Thule Rise is related to the Milne plume [16]. One of the branches of this plume, which was located beneath the axial spreading zone and originated earlier than the Thule Rise, could be a reason for the strong activation of axial magmatism, which led to the formation of the volcanic seamount, the further evolution of which led to the formation of the studied guyot.

## FUNDING

This work was supported by the Russian Science Foundation, project no. 22-27-00036, at the Institute of Geology, Russian Academy of Sciences.

## SUPPLEMENTARY INFORMATION

The online version contains supplementary material available at <https://doi.org/10.1134/S1028334X23602195>.

## CONFLICT OF INTEREST

The authors of this work declare that they have no conflicts of interest.

## OPEN ACCESS

This article is licensed under a Creative Commons Attribution 4.0 International License, which permits use, sharing, adaptation, distribution and reproduction in any medium or format, as long as you give appropriate credit to the original author(s) and the source, provide a link to the Creative Commons license, and indicate if changes were made. The images or other third party material in this article are included in the article's Creative Commons license, unless indicated otherwise in a credit line to the material. If material is not included in the article's Creative Commons license and your intended use is not permitted by statutory regulation or exceeds the permitted use, you will need to obtain permission directly from the copyright holder. To view a copy of this license, visit <http://creativecommons.org/licenses/by/4.0/>

## REFERENCES

1. J. T. Wilson, *Can. J. Phys.* **41**, 863–870 (1963).



2. *General Bathymetric Chart of the Oceans (GEBCO)* (Canad. Hydrogr. Serv., Ottawa, 2004).
3. S. G. Skolotnev, A. A. Peyve, A. N. Ivanenko, et al., *Dokl. Earth Sci.* **504** (1), 233–240 (2022).
4. S. G. Skolotnev, A. A. Peyve, A. Sanfilippo, et al., *Oceanology* **62** (4), 575–578 (2022).
5. O. I. Okina, S. M. Lyapunov, and A. S. Dubensky, *Microchem. J.* **140**, 123–128 (2018).
6. N. M. Sushchevskaya, G. L. Leichenkov, B. V. Belyatsky, and A. V. Zhilkina, *Geochem. Int.* **60** (6), 509–530 (2022).
7. S. S. Sun, R. W. Nesbit, and A. Ya. Sharaskin, *Earth Planet. Sci. Lett.* **96**, 119–133 (1979).
8. R. M. Ellam, *Geology* **20**, 153–156 (1992).
9. A. W. Hoffman, *Earth Planet. Sci. Lett.* **90**, 297–314 (1991).
10. B. L. Weaver, D. A. Wood, J. Tarney, et al., *Geol. Soc. Spec. Publ.*, No. 30, 253–267 (1987).
11. GEOROC Database (Geochemistry of Rocks of the Oceans and Continents) Version 2023-06-01 (2023). <https://georoc.eu/georoc/>.
12. S. R. Hart, *Earth Planet. Sci. Lett.* **90** (3), 273–296 (1988).
13. A. A. Peyve, S. Yu. Sokolov, A. A. Razumovskiy, et al., *Geotectonics* **57** (1), 42–66 (2023).
14. J. G. Schilling, G. Thompson, R. Kingsley, et al., *Nature* **313**, 187–191 (1985).
15. D. Fontignie and J. G. Schilling, *Earth Planet. Sci. Lett.* **146**, 259–272 (1997).
16. R. B. Whitmarsh, A. Ginzburg, and R. C. Searle, *Geophys. J. R. Astron. Soc.* **70**, 79–107 (1982).

*Translated by I. Melekestseva*

**Publisher's Note.** Pleiades Publishing remains neutral with regard to jurisdictional claims in published maps and institutional affiliations.